Application of Atomic Layer Deposition on Ceramic Nanofiltration Membrane

CIE5050-09 Additional Graduation Work

Prepared by
Liying Feng

Supervised by
Dr. ir. Ran Shang
Dr. ir. Bas Heijman

March/2018

Department of Water Management
Faculty of Civil Engineering and Geoscience
Delft University of Technology

Abstract

Pressure driven membranes have become increasingly popular in removal of natural organic matter (NOM). With the purpose to tailor pore size of membrane to remove NOM effectively, atomic layer deposition (ALD) was applied on the ceramic nanofiltration (NF) membrane with a pore size of 1.3 nm. Ceramic membranes were chosen as the substrate membrane due to their high physical strength and high chemical resistance. TiO_2 was deposited on the membrane by using $TiCl_4$ and H_2O as precursors. After deposition with 3 cycles, MWCO of the ceramic membranes was reduced by ~ 250 Da. The pore size of the ceramic membranes was correspondingly narrowed down by ~ 0.16 nm. The growth per cycle of TiO_2 on the pore walls was ~ 0.272 nm/cycle. An improved Carman-Kozeny model was used to estimate water permeability. With the help of two scenarios, the model results are close to the results from water permeability experiments that the water permeability decreased from ~ 24 $L\ h^{-1}\ m^{-2}\ bar^{-1}$ to ~ 6 $L\ h^{-1}\ m^{-2}\ bar^{-1}$. The application of the fabricated membrane in water treatment could be investigated in the further study.

Table of Contents

1 Introduction

Natural Organic Matter (NOM) is a mixture of organic compounds that occur naturally by the degradation of plants and animal bones from soil as well as by-products from microorganism activities (Park et al., 2005). NOM affects water quality in various ways. As a carrier of metals and hydrophobic organic chemicals, NOM is responsible for undesirable odor, color and taste of nature water (Sillanpää et al., 2015). On the other hand, NOM is a source nutrient for heterotrophic bacteria therefore it promotes the re-growth of bacteria in transporting pipes and contributes to the turbidity at the consumer end (Kim et al., 2006). Besides, it reacts with disinfectant and generate Disinfectant By-Products (DBPs) (Uyak et al., 2017).

The physical and chemical properties of NOM vary in time and space. Once the characteristics of NOM have changed, the conventional water treatment processes, including coagulation, sedimentation and filtration, may not meet the criteria. In recent years, pressure driven membranes became more attractive with respect to removal of NOM. Membranes with molecular weight cut-off (MWCO) less than 1000 Da are are required to effectively remove NOM and all pathogens (Winter et al., 2017). In this study, membranes with MWCO in the range from 200 Da to 3000 Da was investigated. Within this range, this kind of membranes are referred to nanofiltration (NF) membranes. The smaller MWCO that membranes have, the higher removal of NOM by membranes can be achieved.

Membrane material can be classified into organic material and inorganic material. Ceramic membrane, also called inorganic membranes, has attracted increasing attention in recent years because of several outstanding characteristics, including high chemical the thermal resistance, long life spans and reclamation potential (Lin, 2002). To fabricate the pore size of ceramic membrane, atomic layer deposition (ALD) has been proved to be an effective technology. According to Shang (Shang et al., 2017), the average active size of ceramic membranes can be reduced from 0.7nm to 0.5nm by using atmospheric pressure atomic layer deposition (APALD). Another studies also demonstrated the successful application of ALD to narrow pore size of ceramic ultrafiltration membranes from 50 nm to around 6.8nm (Li et al., 2012). However, the TiO_2 ALD on ceramic NF membranes in vacuum has not been studied yet. The vacuum condition provides the ALD with a clean environment in the reactor and the effective removal of residual particles (George, 2010). On the other hand, membranes are usually characterized by water permeability and MWCO. The effect of TiO_2 deposition on the water permeability and MWCO of ceramic NF membranes is still not clear. Therefore, the purposes of this work are:

- Understand deposition behavior of TiO2 ALD on ceramic NF membranes in vacuum;
- Investigate the effect of TiO_2 on water permeability and MWCO of ceramic NF membranes.

The characteristics of commercial ceramic membranes including water permeability and MWCO were investigated. The commercial membranes were coated using ALD method to narrow the pore size. After coating the water permeability and MWCO of coated membranes and growth of TiO_2 were measured. The Carmon Kozeny model was used to estimate water permeability of the coated membranes.

2 Background and Theory

2.1 Ceramic Nanofiltration Membrane

Ceramic is a synthetic material made from inorganic materials, such as alumina, titania, zeolite or glassy materials (Mohammad et al., 2012). Ceramic membranes can operate at high temperature, extreme alkalinity or acidity environment and high operating pressure. Ceramic membranes are also distinguished from organic membranes by their long service life and high mechanical strength (Amin et al., 2016).

The structure of ceramic membranes is illustrated in Fig. 2.1 (Induceramic.com, 2018). Typically, the ceramic membrane is composed of multiple layers which are supporting layer, intermediate layer(s) and top layer (Amin et al, 2016). The inner layer is the supporting layer that provides mechanical strength for ceramic membranes. The intermediate layer, which acts as a bridge, is located between the supporting layer and the top layer. Sometimes the intermediate layer is further divided into coarse intermediate layer and fine intermediate layer depending on the pore size of this layer. The top layer, also called separation layer, is the place where the effective separation process happens. Fig. 2.1 shows the cross-flow filtration process. The contaminated water flows through membrane and the pollutants are rejected by the separation layer at the same time. The concentrated stream flows out of membrane while permeate stream flows along the perpendicular direction. The advantage of cross-flow filtration is that the cake layer attached to the membrane surface is flushed away by cross flow, resulting in longer time that a filter unit can be operational.

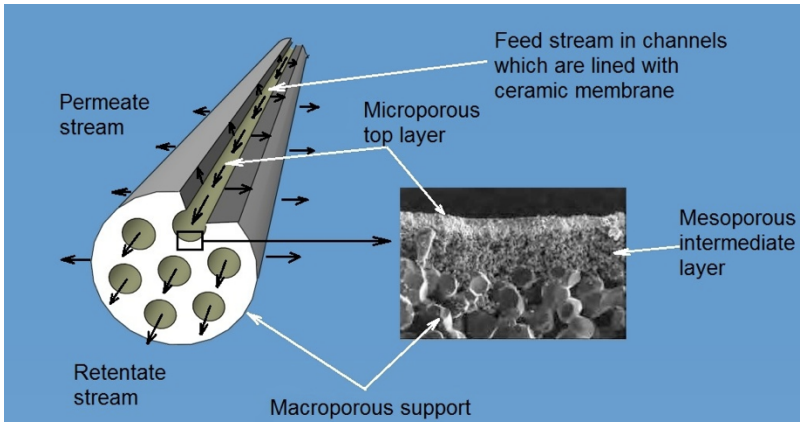

Figure 2.1 Structure of ceramic membrane (Source: http://www.induceramic.com/industrial-ceramic-product/ceramic-membrane)

Ceramic membranes can be categorized by the pore size of the separation layer. The pore size of the separation layer can be reduced to nano-level using fabricating techniques such as sol-gel methods, Chemical Vapour Deposition (CVD) and Atomic Layer Deposition (ALD). Depending on the pore size, ceramic membranes are used for different filtration processes such as ultrafiltration and nanofiltration. Fig. 2.2 shows size of target compounds to be removed and the corresponding filtration processes.

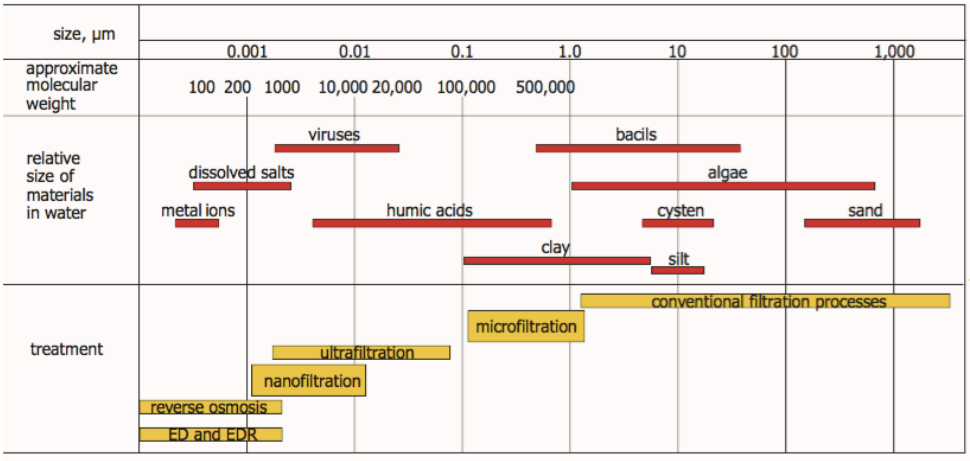

Figure 2.2

(Source: Micro- and ultrafiltration, Drinking Water Treatment, TUDelft)

2.2 Atomic Layer Deposition

Atomic Layer Deposition (ALD) is a technique to deposit thin films to a substrate surface on molecular scale (Koutsonikolas et al., 2017). ALD can be achieved by using different precursors in different operating conditions to deposit the desired thin films on the substrate materials. The flexible mechanism of ALD enable this technique to be used in various applications including semiconductor processing, pore structure tailoring of porous materials and manufacture of high performance of catalyst (Kemell et al., 2008; Van Bui, 2016).

The accurate control of thickness at the monolayer level is one of the most outstanding advantages of ALD. The self-limiting nature of ALD guarantees the process of atomic layer control and deposit a conformal film on the high aspect ratio structure (Lu et al., 2016). Thanks to a purge phase during ALD process, the deposited thin film remains very smoothly and continuously without any pinhole. The only factor that restricts the application of ALD on a large scale is the size of reaction chamber (George, 2010). ALD is usually processed in a vacuum environment therefore a reaction chamber should be big enough to hold the substrates.

Self-limiting surface reaction is the core reaction in ALD process. During the reaction, one precursor chemically reacts with surface spices and deposits a molecule layer on the surface (Leskelä and Ritala, 2002). On the molecule layer there are many surface sites that precursors can react with. As a consequence, the reaction can proceed continuously. Surface reaction proceeds in the gas phase. Fig. 2.3 illustrates the sequence of self-limiting surface reaction during the ALD process.

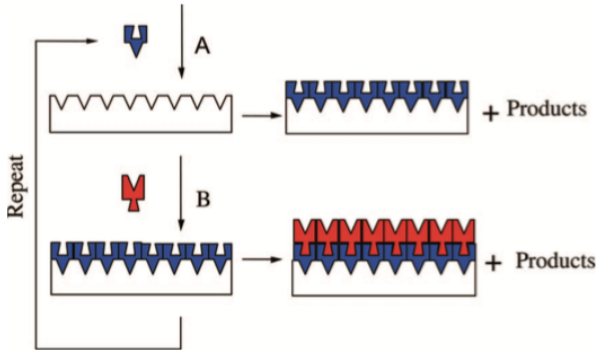

Figure 2.3 Schematic of ALD using self-limiting surface chemistry (George, 2010)

There are several porous materials which can be deposited on the membrane surface by ALD such as Al_2O_3, SiO_2 and TiO_2 (Cameron et al., 2000). In this study, TiO_2 was chosen to be coated on the membrane because it was suggested to be a superior stable material in aqueous solution and had been successfully applied to fabricate porous membranes with the pore size of nano level (Tsuru et al., 2001). The mechanism of deposition is illustrated in Fig. 2.4. Two reactions take place within one cycle. In the first reaction, chlorides replace hydroxyls and Ti-O bonds are formed. Then, H_2O molecules react with chlorides and generate new hydroxyls which will be utilized for further reactions.

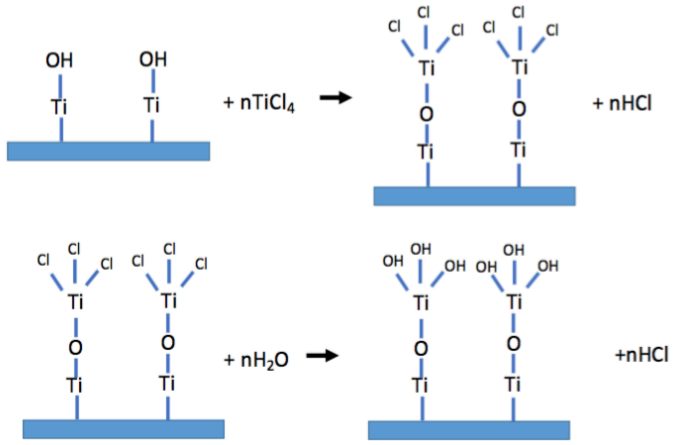

Figure 2.4 Schematic diagram of surface reaction for TiO_2 Atomic Layer deposition using $TiCl_4$ and H_2O.

In the process of ALD, there are various parameters that influence the performance of deposition. They are listed as following and their impacts are discussed.

- Purge time

Purge time should be long enough to remove previous reactants and make reactions occur sequentially and independently on the surface of substrates. If the purge time is not sufficient, Chemical Vapor Deposition (CVD) might happen in the free space in the reacting chamber. In the process of CVD, precursors are present at the same time and react with each other (Tran et al., 2015). If CVD occurs in the chamber, it is more likely to form densely packed particles instead of conformal thin films on the substrates (Kemell et al., 2008). To prevent the formation of packed particles, all the gaseous reagents, including the residual reactants and reaction products, are expected to be removed during the purge time.

- Deposition temperature

Temperature influences the growth of thin film. In Al_2O_3 ALD the growth of Al_2O_3 per cycle decreases with increasing temperature, which is a result of the progressive loss of surface species at high temperature (Ott et al., 1997). In Si ALD, the growth per cycle decreases at low temperature because the surface reaction is not completed. However, temperature should not be too high. Actually, temperature is expected to be set at different values to control the rate of sorption and desorption of precursors in different ALD. The Si ALD is achieved by changing temperature, through which H_2 and $SiCl_2$ desorb sequentially and Si grows on surface

(George, 2010). Overall, the influence of temperature on growth per cycle is different depending on the specific ALD.

- Number of cycles

Theoretically, the thickness of deposited film increases linearly with the increasing number of cycles. In the experiment, however, the thickness is impacted by geometry of the substrate surface. For instance, for porous materials, after a certain number of cycles, precursors cannot diffuse into pores because of the formation of a cover film on the top (Li et al., 2012).

2.3 Scheme of ALD on ceramic membranes

Fig. 2.5 illustrates the coating process of ALD on the cross section of the separation layer of ceramic membranes. In this theoretical model, a thin film forms around ceramic particles so the size of particles increases. Consequently, the distance of two particles reduces and pore size of the separation layer decreases. The thickness of thin film on the top of the separation layer is higher than that on the bottom of separation layer and intermediate layer. In other words, the ceramic particles on the deep layer cannot be coated. The reason for this phenomenon is that precursors are difficult to diffuse into the deep layer. On the other hand, If the coated film connects with each other, there will be a cover on the top that might seal the membrane. To avoid this condition, the coating cycles should be controlled below a certain level.

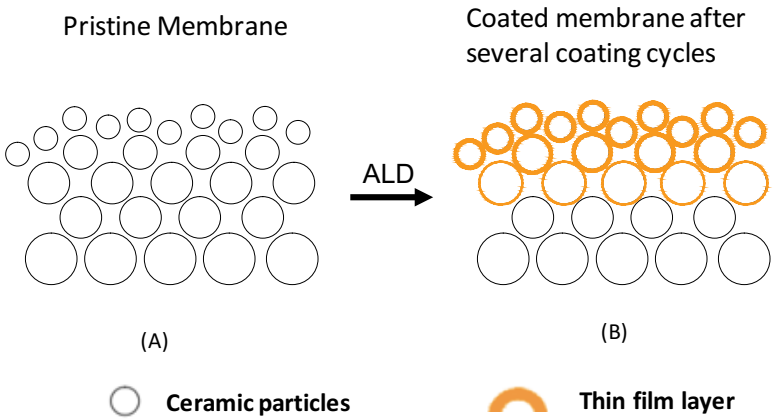

Figure 2.5 Scheme of the pore size tailoring of ceramic membrane by ALD technology

3 Material and Methods

3.1 Substrate Membranes

Two kinds of commercial Nanofiltration (NF) membranes were used as substrate membranes. One of them was produced by Inopor Industry and the other one was produced by Tami Industry. Both of the membranes have effective filtration area of 0.00563m^2. Fig. 3.1 shows the appearance of pristine disc membranes produced by two industries.

Inopor Industry The ceramic NF membranes produced by Inopor Industry (named as LY) has the pronounced mean pore size of 0.9nm and MWCO of 450Da. The supporting layer is made of Al_2O_3 and the separation layer is made of TiO_2 according to the datasheet from Inopor.

Tami industry The ceramic NF membrane produced by Tami Industry (named as MO) has the pronounced MWCO of 1000Da as claimed by the manufacturer. The thickness of the disc membranes is 2.5mm. The supporting layer of the membrane is made of TiO_2 and other layers are made of ZrO_2-TiO_2.

Figure 3.1 Tami Industry ceramic membrane & Inopor Industry ceramic membrane

3.2 Membrane characteristics and performance

3.2.1 Experiment pilot

The purchased membranes were dry before the measurement of permeability and MWCO. The dried membranes were immersed into ultrapure water for more than 8 hours.

Fig. 3.2 shows the schematic overview of experimental equipment used for permeability and MWCO tests. The setup of the equipment was composed by three main parts which were feed water tanks, pump system and cross-flow filtration system. Ultrapure water was used for permeability tests while the Polyethylene Glycol (PEG) solution was used for MWCO tests. The pump system provided desired energy to pump water from one of two tanks to the filtration system. The tested membrane was placed in the membrane holder. Together with pipes linked to tank and pump, they were composed of the cross-flow filtration system. Sensors were installed to measure the cross-flow velocity and the pressure of feed flow and concentrated flow. The temperature meter was put into the feed water tank to measure the instant temperature of the feed water.

The whole system was managed by a software. The software controlled the direction of valves (the bold black line in Fig. 3.2) and the speed of pump. Temperature was shown on screen of the temperature meter.

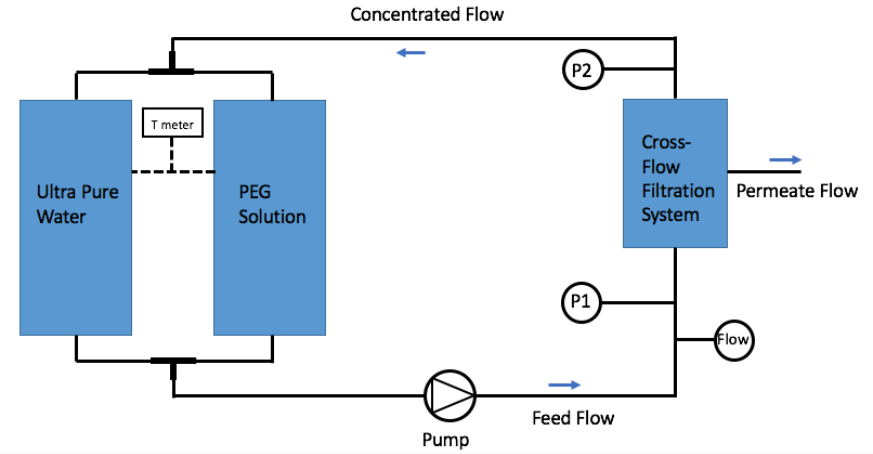

Figure 3.2 Schematic Overview of Experimental Equipment

3.2.2 Water Permeability

Permeability is to evaluate the capacity of membrane to allow the liquid passing from itself under a constant pressure and temperature. The Trans-membrane-pressure (TMP) applied in the permeability test was 3 bar. The velocity of feed flow passing tangentially across the membrane surface, named as membranes cross flow velocity, was adjusted to the rate around 7 m/s. The corresponding flow of the pump was 175 L/h. An Increase of temperature in the feed water was observed during permeability tests because of the heating from operating pump. Temperature was corrected to 20°C by using Eq. 3.1.

$$Lp_{\,20°C} = \frac{J \times e^{-0.0239\,(T-20)}}{P} \qquad Eq.\,3.1$$

$$J = \frac{Q}{A}$$

Where

$Lp_{\,20°C}$: Permeability at 20°C ($\mathrm{L} \cdot h^{-1} \cdot m^{-2} \cdot bar^{-2}$);
J Permeate flux($\mathrm{L} \cdot h^{-1} \cdot m^{-2}$);
T Temperature of the feed solution (°C);
P Pressure applied (bar).
Q Flow rate ($\mathrm{L} \cdot h^{-1}$)
A Effective filtration area (m^2)

The flow rate can be calculated using the following equation.

$$Q = \frac{W_2 - W_1}{\Delta t}$$

W_2 Weight of permeate liquid and beaker (g)
W_1 Weight of empty beaker (g)
Δt Time interval (h)

Then, the temperature-corrected permeability was calculated. The permeability of one membrane was obtained from average value of three parallel tests.

3.2.3 Molecular Weight Cut-Off (MWCO)

- Filtration experiment

Molecular weight Cut-off is an important parameter of membranes. It represents the retention capacity of membranes. MWCO is defined as the molecular weight of tracer material that 90% of which is rejected by membranes. The tracer molecule used in this test was Polyethylene Glycols (PEG). PEG is neutral, therefore the retention of PEG by membrane is a result of steric exclusion rather than electrostatic repulsion. The feed solution was a mixture of PEG with different molecular weight of 200Da, 300Da, 400 Da, 600Da, 1000Da, 1500Da, 2000Da, 4000Da, 6000Da, 8000Da, 10000Da. In the ideal condition, PEG with molecular weight smaller than pore size of membranes passes through while large PEG is rejected. However, pores of membrane can be blocked by large PEG molecule, restricting the passing of smaller PEG molecules. Therefore, the MWCO of membranes is considered to be underestimated in this test.

The concentration of each molecular weight of PEG was 0.6g/L. The previous work done by Shang showed that the concentration of PEG, between 0.2g/L-2g/L for each compound, has no influence on measured MWCO (Shang et al., 2017). The experiment was carried out at applied pressure of 3 bar with pump cross flow of 175 L/h. Temperature was monitored by the temperature meter. The MWCO test was processed under room temperature.

The filtration experiments started with a stabilization period for 90 minutes, followed by sample collection for another 90 minutes. Feed samples and permeate samples were collected at 30-minute intervals. After collection, the feed samples and permeate samples were filtered by 0.45 um filters (Whatman) and then stored in the refrigerator.

- Sample analysis

The permeate solution and feed solution were analyzed by High Performance Liquid Chromatography (HPLC, Shimadzu, Japan) which contains size exclusion chromatography columns (SEC, PSS Polymer Standards Service GmbH, Germany). The feed water with mixture of PEG passed through columns filled with solid adsorbent. PEG with various molecular weight has different traveling velocity when passing through the solid adsorbent, leading to different retention time of each components in the columns. The result shows a peak when a certain PEG flow out of column. The peak position and peak surface area were related to PEG concentration. The retention of PEG can be determined by Eq. 3.2.

$$\mathrm{R}_i = \left(\frac{C_{i,F} - C_{i,P}}{C_{i.F}}\right) \qquad Eq.3.2$$

where
R_i: Retention of PEG with certain molecule weight, -
$C_{i,F}$: PEG concentration in feed solution, g/L
$C_{i,P}$: PEG concentration in permeate solution, g/L

Then a log-normal model was applied mathematically to generate a rejection curve. This curve should be fitted to the molecular weight distribution curve. The MWCO was finally calculated through a function of normal standard inverse.

- Calibration curve

Calibration curve was used to describe the correlation between the elution time (time required to go through the column) and molecular weight of standard samples. The calibration curve was fitted to measured data, and then the molecular weight of tested samples was calculated.

To develop the calibration curve, one need to prepare standard solution. The standard solution contained the PEG having the same concentration as the one used in the filtration experiment (0.6g/L). Each standard solution only contained one molecular weight PEG (i.e. 0.6g/L PEG 300Da, 0.6g/L PEG 600Da, 0.6g/L PEG 1000Da, etc.).

The retention time of each component that presents in the standard solution was obtained by performing the HPLC analysis for all the standard solutions. Then the calibration curve was generated by plotting the measured data of standard samples, which were presented as red dots in Fig. 3.3.

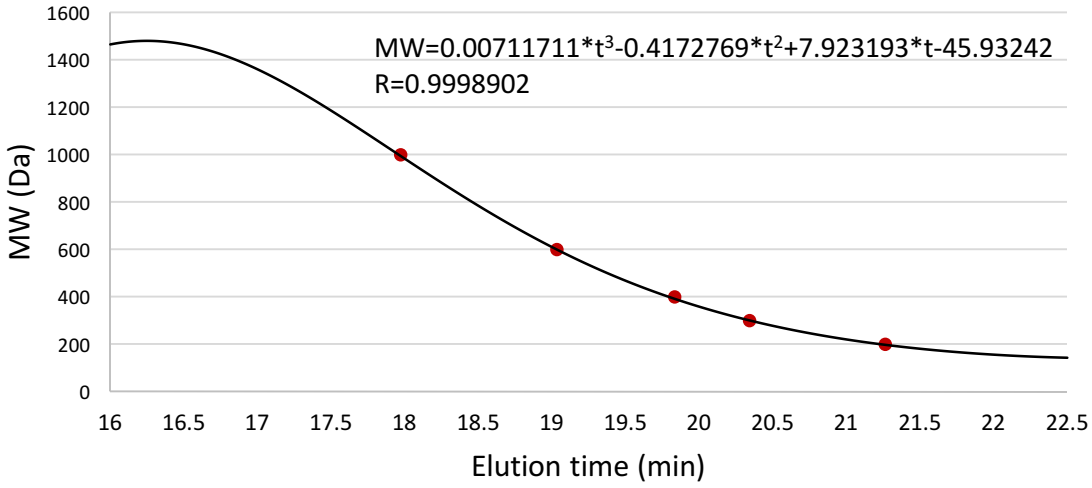

Figure 3.3 calibration curve using PEG with Molecular weight of 200 Da, 300 Da, 400 Da, 600 Da and 1000 Da.

- Defects correction

During the storage (low temperature in refrigerator) and ALD process (High temperature) the pore structure of membrane can be destructed, resulting in defects that influence the analysis result of MWCO. To eliminate the influence of defect on MWCO, a formula was used to correct the measured rejection with defects. The formula is shown as Eq. 3.3.

$$a = \frac{R}{100\% - d} \qquad Eq.\,3.3$$

where
a: Rejection by membrane after correction (%)
R: Measured rejection (%)
d: Defects of membranes (%)

3.2.4 Atomic Layer Deposition

In TiO_2 ALD, $TiCl_4$ and H_2O were used as precursors to coat TiO_2 on the membrane surface. The surface reaction during TiO_2 ALD can be described as the following equations:

$$n(-OH)^* + TiCl_4(g) \rightarrow (-O-)_n(TiCl)_{4-n}{}^* + nCH_4\,(g) \quad (A)$$

$$(-O-)_n(TiCl)_{4-n}{}^* + H_2O(g) \rightarrow (-O-)_nTi(OH)^*_{4-n} + (4-n)HCl(g) \quad (B)$$

where asterisks represent the surface species.

In this process, $TiCl_4$ was primarily exposed to substrate surface and chemicals adsorbed on the surface, forming a monolayer. Next comes to a purge phase, in which the N_2 gas flowed over the surface of the substrate membrane. The purpose of this step is to remove byproducts (HCl) from previous chemical reaction and residual TMA that did not completely react with surface spices. Then, H_2O was introduced to finish one cycle. When one cycle was completed, N_2 purged the reactor again to evacuate the generated CH_4 and residual H_2O. Through the alternating exposure to $TiCl_4$ and H_2O, TiO_2 grew linearly on the substrate surface. All the procedures described above was processed automatically under the vacuum condition at temperature of 180 ℃.

The recipe input into the software was presented in table 3.1 and table 3.2. Due to the changing of laboratory regulation, the TiO2 ALD was switched from one machine to the other during this experiment period and therefore MO membranes were coated by ALD_Oxford while LY membranes were coated by ALD_Ultratech. The similar growth of TiO2 on the surface of silicon wafer was obtained by using the following two recipes on each ALD machine.

Table 3.1 Recipe of TiO2 Deposition for One Cycle in Oxford ALD

Procedure	**time (s)**
$TiCl_4$ pulse	3
$TiCl_4$ purge	30
$TiCl_4$ pump	4
H_2O pulse	3
H_2O purge	30
H_2O pump	2

Table 3.2 Recipe of TiO2 Deposition for One Cycle in Ultratech ALD

Procedure	**time (s)**
$TiCl_4$ pulse	0.2
$TiCl_4$ purge	4
H_2O pulse	0.2
H_2O purge	7

When one cycle was completed, a monolayer of TiO_2 was formed on the surface of the substrate membrane. The number of cycle was set as single variable to investigate the relationship between coating cycles and pore size reduction. Both LY membranes and MO membranes were coated by TiO2 ALD to increase the reproducibility and reliability of coating experiments. Table 3.3 summaries the coating cycles for MO membranes and LY membranes.

Table 3.3 The Coating Cycles for Investigated Membranes

Membrane	**Coating cycles**	**Membrane**	**Coating cycles**
MO4	0	LY 8	0
MO5	5	LY 5	3
MO8	10	LY 6	3

MO10	15	LY 7	3

3.2.5 Thickness of TiO_2

The thickness of the deposited layer was measured by Ellipsometry, which is an optical measurement technique that investigates the dielectric properties of thin layers with the principle of light polarization. Ellipsometry measures the change of polarized light and calculates the thickness by using a dielectric function model (Fujiwara, 2007). However, the direct measurement of thickness of new layer on the membrane surface is difficult since the pore structure of ceramic membrane hinders the reflection of light. To address this issue, a silicon wafer with flat surface was used to determine the thickness of the coated layer. While coating the membrane, the silicon wafer was placed under the membrane. As the wafer is a larger than the membrane, TiO_2 was deposited on the surface of silicon wafer. By measuring the thickness of the wafer before and after coating using the Ellipsometry, the growth per cycle (GPC) was calculated according to Eq. 3.4:

$$\mathrm{GPC} = \frac{d_2 - d_1}{A} \qquad Eq.\,3.4$$

Where

d_2 Thickness of the uncoated wafer, nm

d_1 Thickness of the coated wafer, nm

A Coating cycles, -

4 Result and Discussion

4.1 MO membranes

4.1.1 Growth of TiO2 on silicon wafers by ALD

The growth per cycle (GPC) of TiO_2 on the membrane MO5 (10 cycle) is 0.0382 nm/cycle. The GPC of MO8 and MO10 were not measured due to the stuck issues with the load lock of Oxford ALD. During the experiment the relative position of the wafer and the membrane had changed. To avoid the influence of wafer on the membrane, the small wafer was not put in the chamber while coating MO8 and MO10.

For comparison, the typical GPC for thermal TiO_2 ALD chemistry is 0.04 nm per cycle (Leskelä and Ritala, 2002). In other works depositing TiO_2 on surface of substrates, the GPC ranges from 0.03 to 0.05 nm/cycle (Abdulagatov et al., 2012; Nevalainen et al., 2012; Lei et al., 2013). The different GPC of TiO_2 is attributed to different operating conditions such as temperature, pulse time and purge time (Triani et al., 2006).

4.1.2 Effect of ALD coating on MWCO

Fig. 4.1 shows the defected-corrected MWCO of MO membranes. The reduction of MWCO of coated membranes is inconsistent with the coating cycles. Membrane MO4 is a blank sample that was treated with the same procedure as other membrane except for the ALD process. MO5, MO8 and MO10 were coated with 5 cycles, 10 cycles and 15 cycles respectively. Theoretically, MWCO of MO4 should keep constant before and after coating and the MWCO of the rest three membranes should decrease with increasing number of coating cycles. The irregular result shown in Fig. 4.1 might be attributed to the defects occurred during the experiment process, including transporting, drying, coating and soaking. The defects of each membrane is depicted as blue dots and red dots in the Fig. 4.1. It can be seen that every coated membrane has a certain extent of defect. Among these, the defect of MO 8 and MO 10 are as high as 77.6% and 90.5% respectively. Due to the high defect and inconsistence with expected results, it is impossible to explain the effect of coating on membrane based on the current result from the MO membranes.

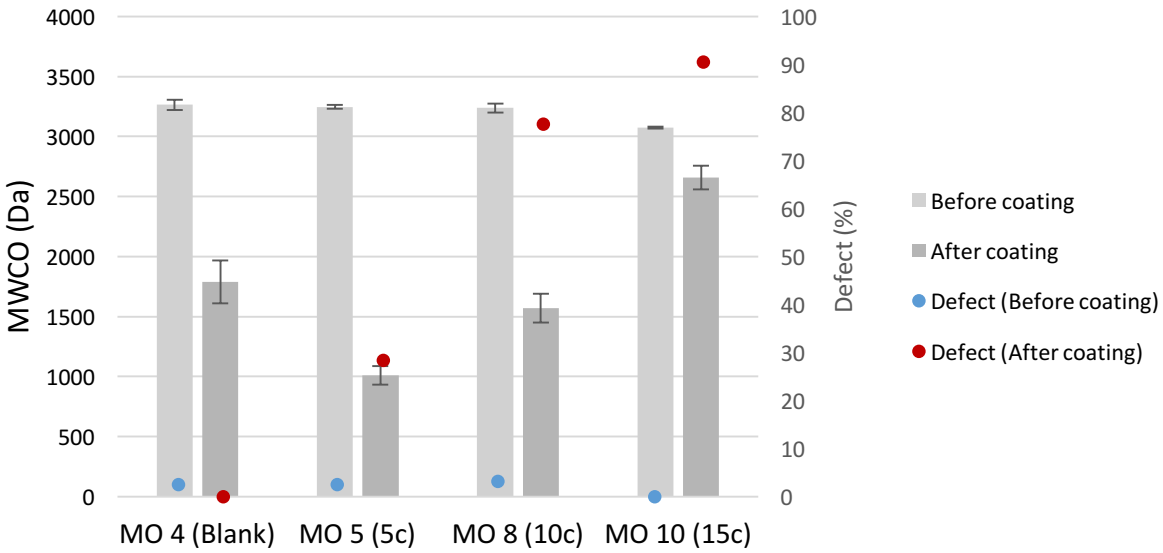

Figure 4.1 Defect-corrected MWCO of MO membrane before and after deposition of TiO2

4.1.3 Effect of ALD coating on permeability

The measured permeability of uncoated and coated MO membranes is shown in Fig. 4.2. Unexpectedly, the decrease of permeability of coated MO5, MO8 and MO10 with increasing coating cycles is not observed here. As described in section 4.1.2, the defects of MO membranes after coating is unpredictably high and this contributes to the unreasonable result in permeability of the coated membranes. If the defects of coated membranes are corrected, the permeability of coated membranes has a reasonable decreasing with the corresponding coating cycles, which is shown in Fig. 4.3.

Again, the membrane matrix is unstable and no conclusion can be drawn regarding to the effect of coating on membrane permeability. The experimental results acquired from MO membranes will no longer be used in the following analysis.

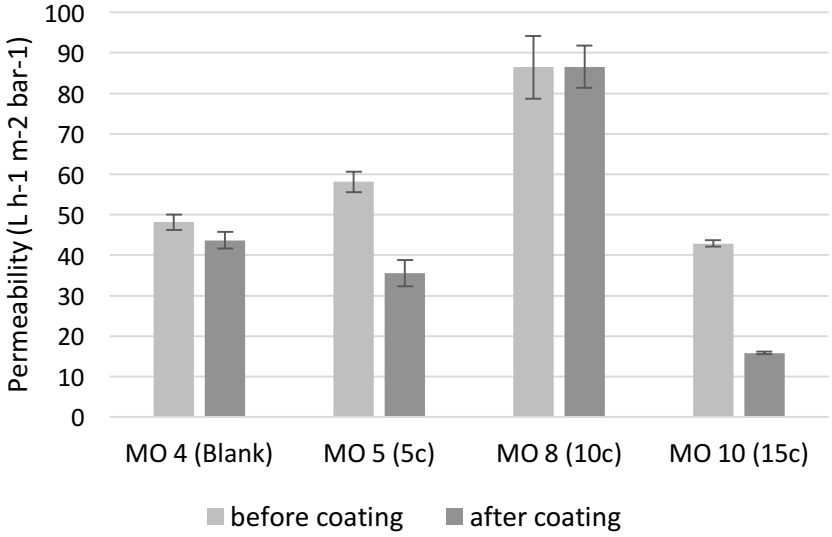

Figure 4.2 Permeability of MO membrane before and after coating of TiO2

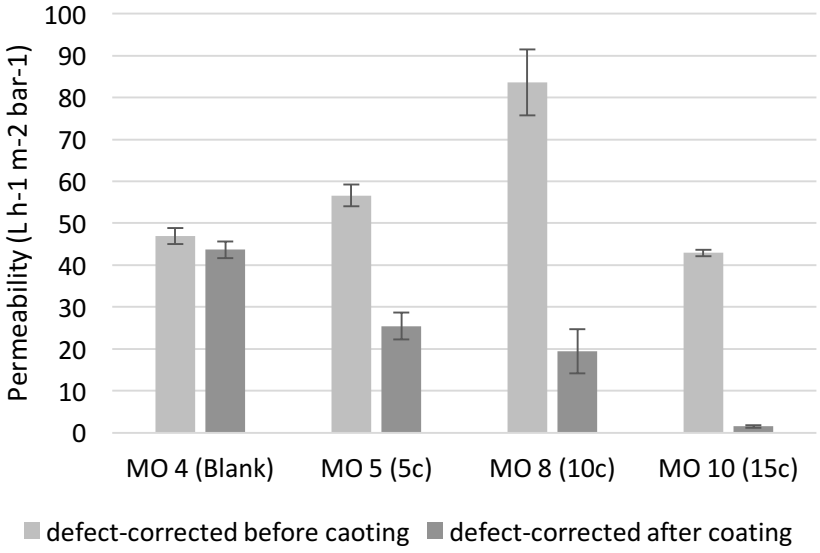

Figure 4.3 Defected-corrected permeability MO membrane before and after coating of TiO2

4.2 LY membranes

4.2.1 Growth of TiO_2 on silicon wafers by ALD

Table 4.1 presents the GPC of TiO_2 on the surface of silicon wafer with the same set of deposition conditions as on the membranes. The average GPC of three silicon wafer is 0.0304±0.053 nm/cycle, which is in agreement with the result in other researches depositing the TiO_2 on the membranes that were stated in Section 4.1.1. Noticeably, there is a deviation of GPC in different deposition experiments. The lowest GPC on wafer surface is 0.0227±0.0028 nm/cycle of the membrane LY6 while the highest one is 0.036±0.0018 of the membrane LY5. It can be explained by the systematic errors such as the slightly different depositing conditions in the chamber and random errors such as the malposition of silicon wafers when it was measured by Ellipsometry before and after deposition of TiO_2.

In addition, the growth of TiO_2on the silicon wafer utilizing ALD_Oxford (0.0382±0.005 nm/cycle) is higher than that on the silicon wafer utilizing ALD_Ultratech (0.0304±0.007 nm). It would be ascribed to that longer pulse time for each precursor used in the Oxford recipe allows more precursors to be adsorbed on the surface and produce more amount of TiO_2 in each cycle (Chen et al., 2017).

Table 4.1 GPC of TiO_2 on Surface of Silicon Wafers by ALD_Ultratech

Membrane	**LY 5 (3c)**	**LY 6 (3c)**	**LY 7 (3c)**	**LY 8 (blank)**
GPC (nm/cycle)	0.036	0.0227	0.0327	0
Avg. GPC (nm/cycle)		0.0304		

It was worth noting that the GPC reported in this study was measured on the surface of silicon wafers rather than on walls of inner pores of the membranes. The GPC on the walls of inner pore can be derived from the change of pore size and the pore size can be estimated by Eq. 4.1.

$$D = 0.065(MWCO)^{0.438} \qquad Eq.\,4.1$$

Where

D Diameter of pore size in filtration layer, nm

$MWCO$ Molecular weight cut-off of ceramic membranes, Da

Table 4.2 GPC on Walls of Inner Pores Estimated from MWCO

Membrane	**LY 5 (3c)**	**LY 6 (3c)**	**LY 7 (3c)**	**LY 8 (blank)**
GPC (nm/cycle)	0.0302	0.0263	0.0250	0
Avg. GPC (nm/cycle)		0.0272		

The average GPC on the surface of silicon wafer is very close to that on the wall of inner pores. It is because two substrate materials have similar surface chemistry and hydroxyl groups (Chen et al., 2018). The predicable GPC is beneficial for precise control of pore size.

4.2.2 Effect of ALD coating on MWCO

The effect of ALD coating on the MWCO of membranes was investigated through parallel experiments. All the membranes LY5, LY6 and LY7 were coated with 3 cycles to increase the reproducibility of this work. The membrane LY8 was treated as a blank sample that was not deposited. Fig. 4.4 shows the reduction of MWCO of three deposited membranes (LY5, LY6 and LY7) and almost constant MWCO of the blank membrane (LY8). With 3 cycles, the MWCO of the membrane LY5 decreased from 726±33 Da to 493±14 Da, whereas that of the membrane LY 6 was tightened from 919±90 Da to 683±7 Da. The membrane LY7 exhibits a similar reduction of MWCO about 250 Da from 1060±48 Da to 813±24 Da. Although the three pristine membranes have various pore size, the reduction of MWCO after deposition is close to each other, indicating that the effect of ALD on pore size is independent of original pore size.

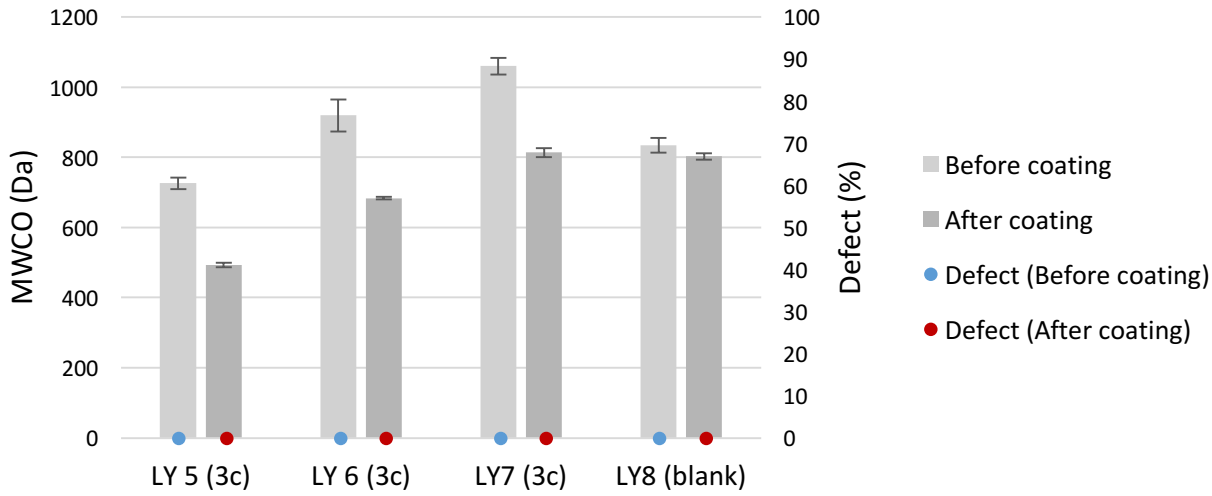

Figure 4.4 MWCO of LY membrane before and after deposition of TiO2

As the blank membrane keeps the same MWCO after deposition (the small variation of MWCO of LY8 is negligible), it can be concluded that the decrease of MWCO is only attributed to the deposition process. According to Eq. 4.1, the MWCO and pore size of the measured membranes are positively correlated. This result indicates that the pores in separation layer of ceramic membranes can be effectively tuned by ALD.

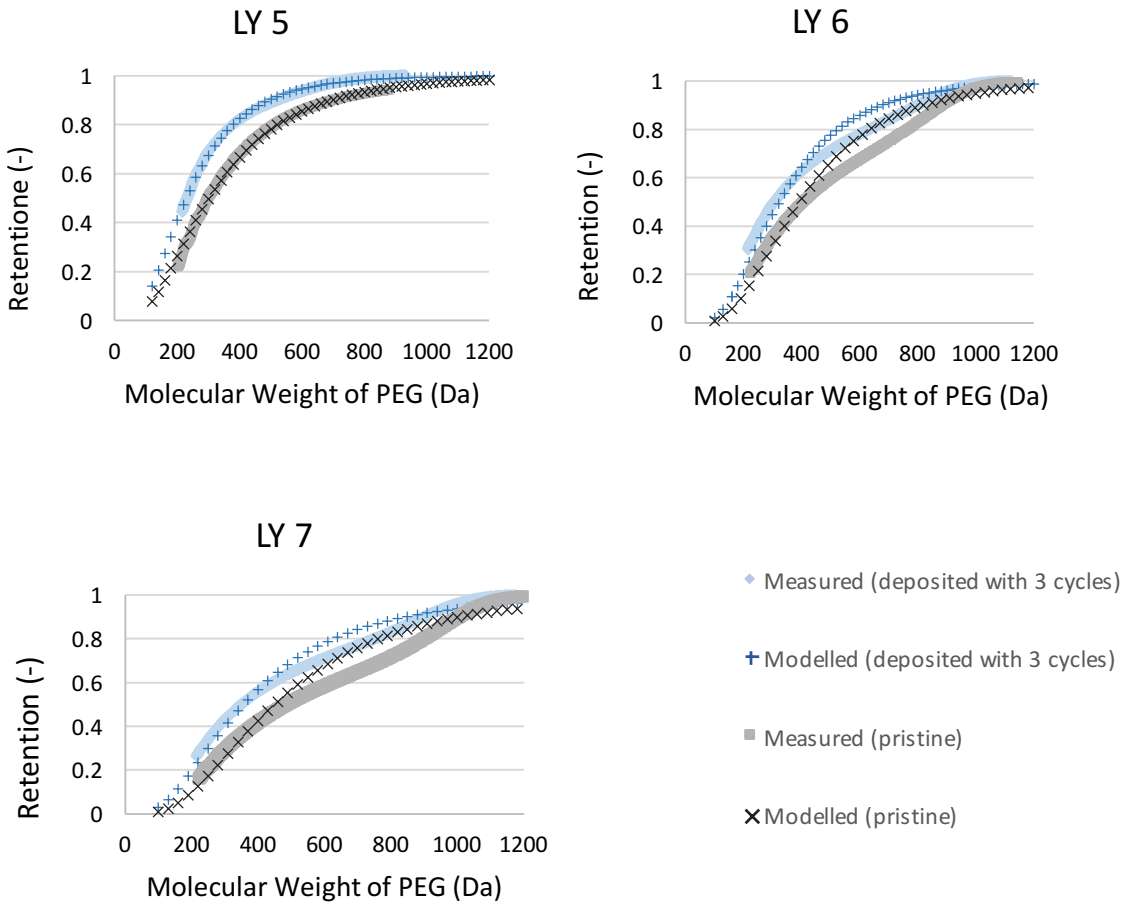

Figure 4.5 PEG retention of membranes LY 5, LY 6 and LY 8 before and after deposition

The rejection performance of deposited membranes was investigated by measuring the MWCO utilizing the PEG with different molecular weight. Fig. 4.5 exhibits the rejection of PEG as a function of MWCO in 3 deposited membranes. The result illustrates that the ALD route successfully improved the rejection performance of the measured ceramic NF membranes.

4.2.3 Effect of ALD coating on water permeability

Water permeability was measured on the pristine and deposited membranes at room temperature, and the result is depicted in the Fig. 4.6. As shown in Fig 4.6, before coating, water permeability of the membrane LY5 is 24.62±0.21 L/(hm^{2}bar) and decreases to 4.57±0.13 L/(hm^{2}bar) after coating. The other coated membranes LY6 and LY7 also exhibit a reduction of water permeability after deposition of TiO_2. It is due to the reduction of pore size by the newly formed TiO_2 layer deposited on the pore walls and thus the water transport resistance increases correspondingly. Unexpectedly, the blank membrane LY8 shows an incremental permeability compared to the pristine one. Considering that the MWCO of membrane LY8 was unchanged before and after deposition, the increased permeability is attributed to the measuring errors. In Section 4.2.4, a mathematical model is developed to mimic the permeability obtained from measurement.

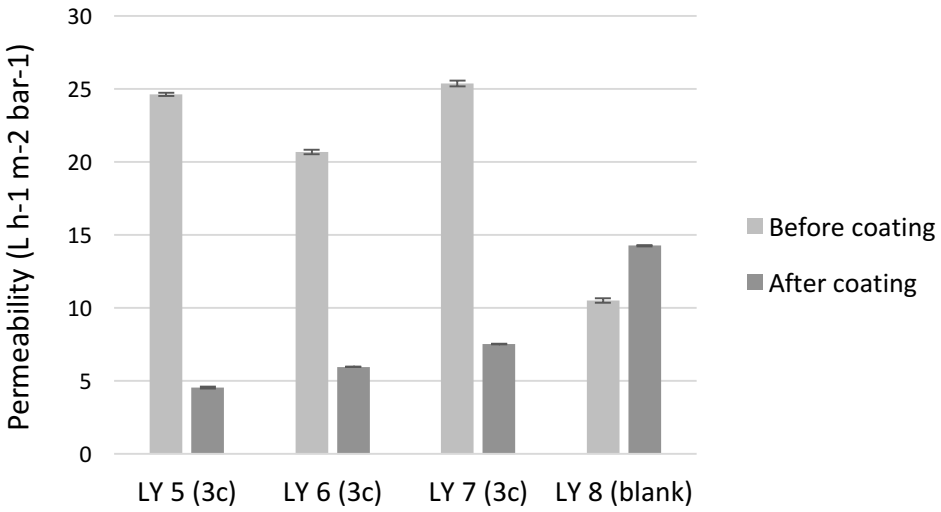

Figure 4.6 Permeability of LY membrane before and after deposition of TiO2

5 Carman-Kozeny Model

5.1 Introduction and Equations

Carman-Kozeny equation, which was firstly derived by Josef Kozeny and Philip C. Carman, is commonly used to predict permeability for granular porous media by modelling fluid flow through a packed bed of solid (Khabbazi et al., 2013). It was then improved by Hagen to address the restriction in Carman-Kozeny equation that the pore has to be cylindrical and straight (Seader et al., 1998; Ergun, 1952). The modified equation (Eq. 5.1) therefore validates the Carman-Kozeny approach to estimate flux through porous materials in a more precise way. In current work, this modified Carman-Kozeny Model was applied to estimate ultrapure water permeability. The simulation results were compared with the measured results from the water permeability experiment.

$$J = \frac{\rho \varepsilon^3 \Delta P}{2(1-\varepsilon)^2 \tau a_v^2 \mu l} \qquad Eq.\,5.1$$

where

J flux through membrane, $m^3/(m^2 \cdot s)$
ρ density of the fluid, kg/m^3
ε porosity of membrane, -
ΔP transmembrane pressure, pa
τ tortuosity factor, -
a_v specific surface area, $1/m$
μ viscosity of the fluid, $pa \cdot s$
l layer thickness, m

5.2 Two-layer model

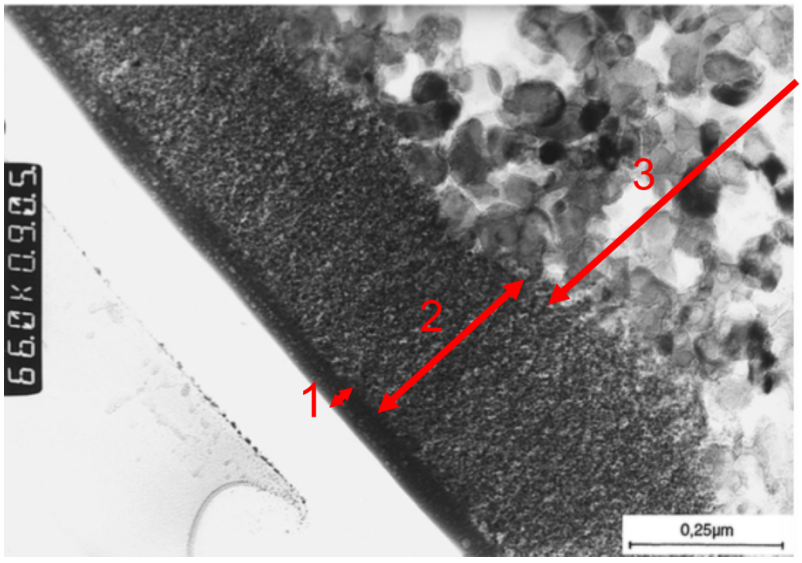

Figure 5.1 SEM cross section of pristine TiO2 membrane with MWCO of 480 Da. 1: Separation layer. 2: Intermediate layer. 3: coarse intermediate layer (Puhlfürß, et al., 2000)

Fig. 5.1 shows scanning electron microscope (SEM) micrograph of an Inopor membrane on the cross section of top multi-layer (Puhlfürß et al., 2000). According to the supplier, in the pristine membrane the pore size of intermediate layer beneath the separation layer (layer 2: 3nm) approaches to the pore size of separation layer (layer 1: around 1.2nm). It can be deduced that both of the separation layer and the intermediate layer predominate the permeate flux.

To calculate the total flux, the separation layer and the intermediate layer were considered separately because the porosity and pore size are different in both layers. The difference of porosity and pore size results in different resistance in each layer, which can be added together by using resistance-in-series model. The total resistance is related to permeate flux. In the end, the total flux can be derived. The deriving process is shown below.

$$R_{total} = R_s + R_m$$

$$\mathrm{R} = \frac{\Delta P}{J \cdot \mu}$$

$$J_{total} = \frac{J_s \cdot J_m}{J_s + J_m} \qquad Eq.\,5.2$$

where
J_s permeate flux in separation layer, $m^3/(m^2 \cdot s)$
J_m permeate flux in intermediate layer, $m^3/(m^2 \cdot s)$
R_s resistance in separation layer, m^{-1}
R_m resistance in intermediate layer, m^{-1}

The permeate flux is converted to permeability by multiplying with membrane surface area as shown in Eq. 5.3.

$$L = J \times A \times 3600 \times 10^5 \qquad Eq.\,5.3$$

5.3 Assumptions and Scenarios

Several assumptions have been made in the Carman-Kozeny model to estimate water permeability. They were listed as following:

1. The test of ultrapure water permeability was performed at room temperature (around 20 °C) and atmospheric pressure (101 325 Pa). Therefore, the density and viscosity of the fluid (water) are 998.19 kg/m^3 and 0.0010016 $pa \cdot s$ respectively.

2. The porosity of the pristine membrane was firstly estimated to be 0.3 in both the separation layer and intermediate layer according to the Inopor membrane specification (Inopor, 2015). The porosity of the coated membranes was calculated by using Eq. 5.4.

$$\frac{\varepsilon_{coated}}{\varepsilon_{pristine}} = \left(\frac{D_{coated}}{D_{pristine}}\right)^3 \qquad Eq.\,5.4$$

where
D pore size, nm

3. For the porous materials, the tortuosity is expressed as a function of porosity. Eq. 5.5 (Meredith and Tobias, 1962) was suggested to be a good estimation for tortuosity in most types of porous materials (Pisani, 2009).

$$\tau = \varepsilon^{-0.5} \qquad Eq.5.5$$

4. The correlation between specific surface area (a_v) and hydraulic diameter (D) of membranes is described in Eq. 5.6 (Seader et al., 1998), where D can be calculated by Eq. 4.1 in Section 4.2.1.

$$a_v = \frac{4\varepsilon}{D \cdot (1-\varepsilon)} \qquad Eq.5.6$$

5. The layer thickness of separation layer and intermediate layer were firstly estimated by measuring the length of each layer on Fig. 5.1. The average thickness of separation layer is 50 nm whereas that of intermediate layer is 320 nm.

6. The coating depth was estimated by Knudsen diffusion model which describes a mean of diffusion in small pores when the involved particles collide frequently against narrow and long pore wall (Malek and Coopens, 2003). The Knudsen diffusion model can be written as Eq. 5.7:

$$\mathrm{Q}_K = \frac{\Delta P d^3}{6 l_e P_{ave}} \sqrt{\frac{2\pi RT}{M_A}} \qquad Eq.5.7$$

Where Q_K is the volumetric flow rate in m^3/s, d is pore diameter in m, M_A is molecular mass (kg/mol), ΔP is the pressure difference between both side of the pore, P_{ave} is absolute pressure in the system , l_e is the effective length of pores which can be subtitled as $l + \frac{4}{3}d$, T is temperature in K, R is gas constant 8.3144 $J/(mol \cdot K)$.

When membranes with various pore size are coated in a certain deposition condition, all the parameters except d are the same. The unchangeable parameters are simplified into one constant parameter B in the Eq. 5.8.

$$\mathrm{Q}_K = B \cdot \frac{d^3}{l+d} \qquad Eq.5.8$$

It is assumed that the membrane pores are cylinder-shaped and the diameter of cylinder is equal to the pore diameter. Then, the coating rate can be derived form Eq. 5.8 (The unchangeable parameter is regarded as C in Eq. 5.9).

$$h_v = \frac{Q_K}{A} = \frac{4Q_K}{\pi d^2} = \frac{d}{C+d}$$

$$\frac{1}{h_v} = 1 + C \cdot \frac{1}{d} \qquad Eq.5.9$$

The reciprocal of flow rate is linearly related to reciprocal of pore diameter. Together with experimental result from Li (Li, 2018) who also performed the thermal ALD for TiO_2 deposition on ceramic membranes, the coating depth in this study is estimated to be about 100nm. It is deeper than separation layer but shallower than intermediate layer. To simply the calculation, both layers were assumed to be fully coated.

Thickness-Variety Scenario

A Thickness-Variety Scenario was used to investigate the model sensitivity to layer thickness and to estimate the thickness of separation layer of the coated membranes.

In the Thickness-Variety Scenario, the variable is the thickness of separation layer that changes from 50 nm to 120 nm. The fixed parameters (density and viscosity of the fluid, tortuosity and porosity of the membrane, specific surface area) were estimated following the assumptions described in Section 5.3. The TMP was measured in the water permeability experiments. The variable and fixed parameters used in the thickness-variety scenario are summarized in the Appendix A.

Porosity-Variety Scenario

Since pores size is not evenly distributed in the membrane, the porosity of the investigated membrane may not be 0.3 as provided by suppliers. Here, the Porosity-Variety Scenario was used to investigate the model sensitivity to porosity and to estimate the porosity of separation layer.

In the Porosity-Variety Scenario, the variable is the porosity of separation layer that changes from to 0.1 to 0.3. The fixed parameters (density and viscosity of the fluid, tortuosity, thickness of the separation layer, specific surface area) were estimated following the assumptions described in Section 5.3. The TMP was measured in the water permeability experiments. The variable and fixed parameters used in the porosity-variety scenario are summarized in Appendix B.

5.4 Result and discussion

5.4.1 Thickness-Variety Scenario

Fig. 5.2 and Fig. 5.3 show the model results that water permeability is a function of the thickness of separation layer. When the thickness of separation layer increases from 50nm to 120nm, the permeability of pristine membranes decreases about 40% according to the model result (Fig. 5.2). It can be logically explained by the increased transport resistance in the thicker layer which results in lower permeate flux.

The measured permeability of coated membranes is shown as dot lines in two Fig. 5.2 and Fig. 5.3. For the membrane LY 5, the dot line (measured permeability) intersects with solid line (model permeability) and the X value of intersect point is the estimated layer thickness by the model. The procedure was repeated for the membranes LY 6 and LY 7. The average value of the estimated layer thickness from LY5, LY6 and LY7 is considered as the the thickness of the separation layer for Inopor NF membranes. The result shows that the separation layer is 88nm for the uncoated membranes and is 199nm for the coat membranes. This result is confirmed by Table 5.1 where the modeling result and the measured result approach to each other. This thickness is different from the given thickness of separation layer which is 50 nm.

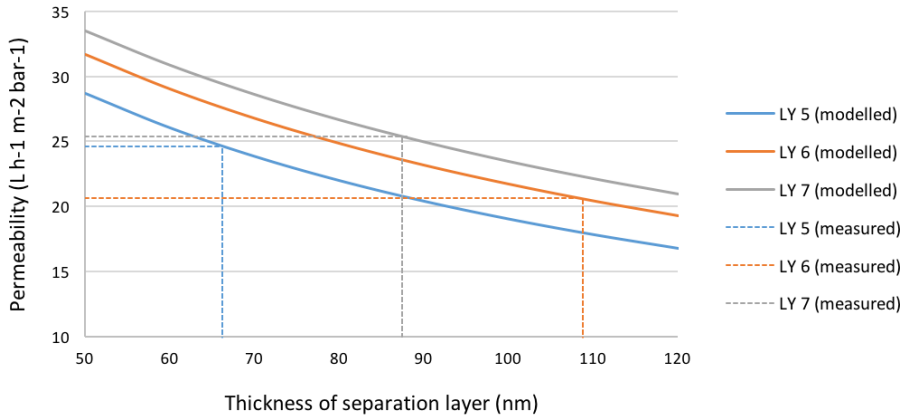

Figure 5.2 Result of Thickness-Variety Scenario for pristine membranes

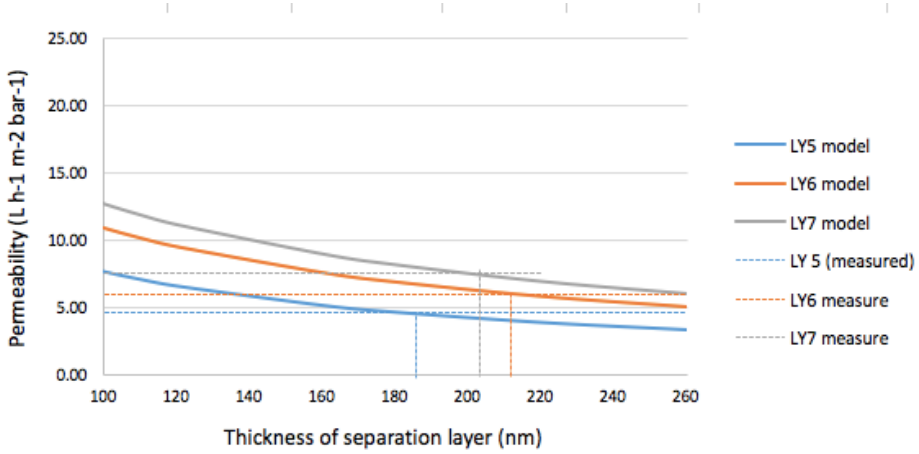

Figure 5.3 Result of Thickness-Variety Scenario for coated membranes

Table 5.1 Modeling Water Permeability ($L/(h \cdot m^2 \cdot bar)$) Using the Estimated Thickness of Separation Layer and the Measured Result from Water Permeability Experiments

	Before coating (estimated thickness: 88nm)			**After coating (estimated thickness: 199nm)**		
	LY5	LY6	LY7	LY5	LY6	LY7
Model Permeability	20.67	23.51	25.28	4.21	6.30	7.55
Measured Permeability	24.62	20.66	25.37	4.57	5.96	7.53

5.4.2 Porosity-Variety Scenario

The result of Porosity-Variety scenario indicates that the porosity of separation layer positively influences on the permeability. It is because that larger void space allows more water to flow through the membrane in the certain period of time. The model permeability is in agreement with the measured permeability when the porosity of separation layer is 0.21 for the uncoated membranes (Fig. 5.4) and 0.26 for the coated membranes (Fig. 5.5). Table 5.2 shows the model results by using the average porosity of 0.21.

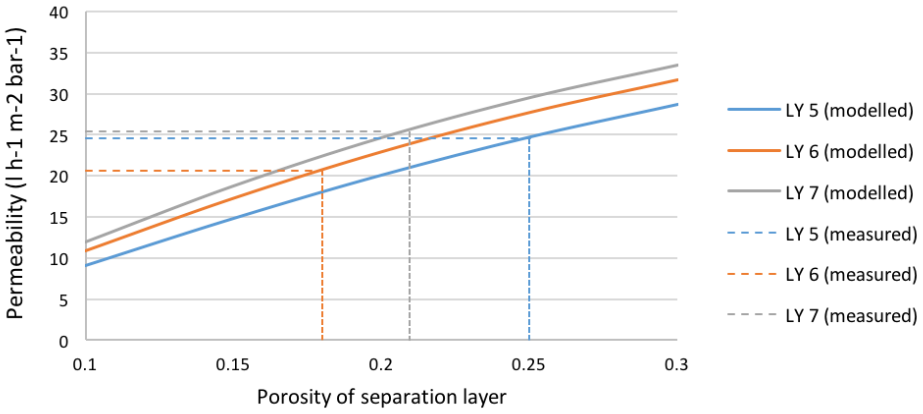

Figure 5.4 Result of Porosity-Variety Scenario for pristine membranes

Table 5.2 Model Water Permeability ($L/(h \cdot m^2 \cdot bar)$) Using the Estimated Porosity of Separation Layer and Measured Result from Water Permeability Experiments

Porosity: 0.21	**Before coating**			**After coating**		
	LY5	LY6	LY7	LY5	LY6	LY7
Modeling result	21.08	23.94	25.72	8.63	12.18	14.11
Measured result	24.62	20.66	25.37	4.57	5.96	7.53

5.5 Limitations

5.5.1 Limitations in Thickness-Variety scenario

In the thickness-variety scenario, the model thickness of separation layer fits less well on pristine membranes. In reality, there is no clear boundary between the separation layer and intermediate layers. The two-layer model used in this study is only an idealized model with the purpose to simplify the calculation. Compared with pristine membranes, the model result has a better match with experimental results from coated membranes. In this model, although the coating depth of TiO_2 on top multi-layer was not measured, an assumption that both of the separation layer and intermediate layers have been coated after deposition was made. With this assumption, the good match of model results and measured results was observed.

5.5.2 Limitations in Porosity-Variety scenario

Though the estimated porosity 0.21 was applied in the Carman-Kozeny model, the model permeability still deviates from the measured one. One possible reason for the deviation is that the pores are not homogeneous in the pristine membranes and some small pores in the separation layer are sealed during deposition. The sealed pores influenced the permeability, however, it was not considered in the model. It is difficult to describe the inherent structure and geometry properties of porous materials in the Carman-Kozeny model, which increases the uncertainties of model results.

5.5.3 Limitations in Carman-Kozeny model

Apart from the limitations mentioned above, the applied model in current work contains many other limitations. One of them is that this model estimates the fluid flows through a packed bed of solids following the laminar flow (Henderson, 2010). However, the ceramic particles are not well packed. It may cause deviation between measured results and model results. Besides, both scenarios only simulate the thickness and porosity of separation layer but take intermediate layer out of consideration. One can expect more accurately simulating result if intermediate layer is included in scenarios.

Although there are some uncertainties, the permeability predicted by Carman-Kozeny model still matches with experimental results with the application of two scenarios. The parameters filled in this model provide a basic estimation of permeability for the Inopor membranes with MWCO less than 1000 Da.

6 Conclusion and Recommendations

The purpose of this study is to investigate the influence of ALD on ceramic nanofiltration membrane with respect to permeability and MWCO. Substrate membranes from two companies were used in this study. For Tami membranes, the irregular and unpredictable results indicate that Tami membranes have much defects. Unlike Tami membranes, the Inopor membranes exhibited stable properties therefore only the results from Inopor membranes were analysed.

In this study, TiO_2 was deposited by ALD on the ceramic nanofiltraiton membranes which have MWCO from 700 Da to 1000 Da. The experimental results confirmed that the pore size of ceramic membranes decreased after deposition of TiO_2 and the pore size was precisely controlled. Tuned by ALD, the deposited membranes showed decreased water permeability and increased rejection of PEG. Afterwards, an improved Carman-Kozeny model was applied to estimate the water permeability of the ceramic membranes in a numerical way. With the help of two scenarios, the model successfully estimated the real permeability obtained from experiments even though some restrictions still existed in this model.

In the further study, it is recommended to use SEM to explore the structure of pores and the thickness of each layer so that it can be compared with the one found in the model scenarios. Besides, the ceramic membranes can be coated with more cycles to reach the smaller pore size.

Bibliography

Abdulagatov, AI, Hall, RA, Sutherland, JL, Lee, BH, Cavanagh, AS, & George, SM (2012). Molecular layer deposition or titanic films using TiCl4 and ethylene glycol or glycerol: growth and properties. *Chemistry of Materials*, *24* (15), 2854-2863.

Amin, S. K., Abdallah, H. A. M., Roushdy, M. H., & El-Sherbiny, S. A. (2016). An overview of production and development of ceramic membranes. *International Journal of Applied Engineering Research*, *11*(12), 7708-7721.

Cameron, M. A., Gartland, I. P., Smith, J. A., Diaz, S. F., & George, S. M. (2000). Atomic layer deposition of SiO2 and TiO2 in alumina tubular membranes: pore reduction and effect of surface species on gas transport. *Langmuir*, *16*(19), 7435-7444.

Chen, H., Wu, S., Jia, X., Xiong, S., & Wang, Y. (2018). Atomic Layer Deposition Fabricating of Ceramic Nanofiltration Membranes for Efficient Separation of Dyes from Water. *AIChE Journal*.

Chen, H., Jia, X., Wei, M., & Wang, Y. (2017). Ceramic tubular nanofiltration membranes with tunable performances by atomic layer deposition and calcination. *Journal of Membrane Science* , *528* , 95-102.

Ergun, S. (1952). Mass-transfer rate in packed columns-its analogy to pressure loss. *Chemical Engineering Progress*, 48(5):227–236.

George, S. M. (2010). Atomic layer deposition: an overview. *Chem. Rev*, *110*(1), 111-131.

Henderson, N., Brêttas, J. C., & Sacco, W. F. (2010). A three-parameter Kozeny–Carman generalized equation for fractal porous media. *Chemical Engineering Science*, *65*(15), 4432-4442.

Kemell, M., Ritala, M., Leskelä, M., Groenen, R., & Lindfors, S. (2008). Coating of highly porous fiber matrices by atomic layer deposition. *Chemical Vapor Deposition*, *14*(11-12), 347-352.

Khabbazi, A. E., Ellis, J. S., & Bazylak, A. (2013). Developing a new form of the Kozeny–Carman parameter for structured porous media through lattice-Boltzmann modeling. *Computers & Fluids*, *75*, 35-41.

Kim, HC, Yu, MJ, & Han, I. (2006). Multi-method study of the characteristic chemical nature of aquatic humic substances isolated from the Han River, Korea. *Applied geochemistry*, 21(7), 1226-1239.

Koutsonikolas, D. E., Kaldis, S. P., & Pantoleontos, G. T. (2017). Preparation of Silica Membranes by Atomic Layer Deposition. In *Current Trends and Future Developments on (Bio-) Membranes*(pp. 45-62).

Lei, Y., Lu, J., Zhao, H., Liu, B., Low, K., Wu, T., Libera, J., Greeley, J., Chupas, P., Miller, J. and Elam, J. (2013). Resolving Precursor Deligation, Surface Species Evolution, and Nanoparticle Nucleation during Palladium Atomic Layer Deposition. *The Journal of Physical Chemistry C*, 117(21), 11141-11148.

Leskelä, M., & Ritala, M. (2002). Atomic layer deposition (ALD): from precursors to thin film structures. *Thin solid films* , *409* (1), 138-146.

Li, F., Yang, Y., Fan, Y., Xing, W., & Wang, Y. (2012). Modification of ceramic membranes for pore structure tailoring: The atomic layer deposition route. *Journal of membrane science*, *397* , 17-23.

Li, F., Li, L., Liao, X., & Wang, Y. (2011). Precise pore size tuning and surface modifications of polymeric membranes using the atomic layer deposition technique. *Journal of membrane science*, *385*, 1-9.

Lin, Y. S., Kumakiri, I., Nair, B. N., & Alsyouri, H. (2002). Microporous inorganic membranes. *Separation and Purification Methods*, 31(2), 229-379.

Li, J. (2018). Plasma-enhanced Atomic Layer Deposition for Synthesis of ceramic Tight UF membrane. Master Thesis Report.

Lu, J., Elam, J. W., & Stair, P. C. (2016). Atomic layer deposition—sequential self-limiting surface reactions for advanced catalyst "bottom-up" synthesis. *Surface Science Reports*, *71*(2), 410-472.

Malek, K. and Coppens, M.O., 2003. Knudsen self-and Fickian diffusion in rough nanoporous media. *The Journal of chemical physics*, *119*(5), pp.2801-2811.

Merdith, R. E. (1962). Conduction in heterogeneous systems. *Advances in electrochemistry and electrochemical engineering*, *2*, 17-48.

Mohammadi, T., & Maghsoodlorad, H. (2013). Synthesis and Characterization of Ceramic Membranes (W-Type Zeolite Membranes). *International Journal of Applied Ceramic Technology*, *10* (2), 365-375.

Nevalainen, K., Isomäki, N., Honkanen, M., Suihkonen, R., McNally, T., Harkin-Jones, E., Syrjälä, S., Vuorinen, J. and Järvelä, P. (2011). Melt-compounded nanocomposites of titanium dioxide atomic-layer-deposition-coated polyamide and polystyrene powders. *Polymers for Advanced Technologies*, 23(3), 357-366.

Ott, A. W., Klaus, J. W., Johnson, J. M., & George, S. M. (1997). Al 3 O 3 thin film growth on Si (100) using binary reaction sequence chemistry. *Thin Solid Films*, *292*(1), 135-144.

Park, N., Kwon, B., Sun, M., Ahn, H., Kim, C., Kwoak, C., Lee, D., Chae, S., Hyung, H. and Cho, J. (2005). Application of various membranes to remove NOM typically occurring in Korea with respect to DBP, AOC and transport parameters. *Desalination*, 178(1-3),161-169.

Pisani, L. (2011). Simple expression for the tortuosity of porous media. *Transport in Porous Media* , *88* (2), 193-203.

Puhlfürß, P., Voigt, A., Weber, R., & Morbé, M. (2000). Microporous TiO2 membranes with a cut off< 500 Da. *Journal of Membrane Science*, *174*(1), 123-133.

Seader, J. D., Henley, E. J., and Roper, D. K. (1998). Separation process principles.

Shang, R., Goulas, A., Tang, C. Y., de Frias Serra, X., Rietveld, L. C., & Heijman, S. G. (2017). Atmospheric pressure atomic layer deposition for tight ceramic nanofiltration membranes: Synthesis and application in water purification. *Journal of Membrane Science*, *528*, 163-170.

Sillanpää, M. (2014). *Natural organic matter in water: Characterization and treatment methods*. Butterworth-Heinemann.

Song, Z., Fathizadeh, M., Huang, Y., Chu, K., Yoon, Y., Wang, L., Xu, W. and Yu, M. (2016). TiO 2 nanofiltration membranes prepared by molecular layer deposition for water purification. *Journal of Membrane Science*, 510, 72-78.

Tsuru, T., Hironaka, D., Yoshioka, T., & Asaeda, M. (2001). Titania membranes for liquid phase separation: effect of surface charge on flux. *Separation and Purification Technology*, *25*(1), 307-314.

Triani, G., Evans, P., Attard, D., Prince, K., Bartlett, J., Tan, S. and Burford, R. (2006). Nanostructured TiO2 membranes by atomic layer deposition. *Journal of Materials Chemistry*, 16(14), p.1355.

Tran, DT, Thieffry, G., Jacob, M., Batiot-Dupeyrat, C., & Teychene, B. (2015). Modification of tubular ceramic membranes with carbon nanotubes using catalytic chemical vapor deposition. *Water Science and Technology* , *72* (8), 1404-1410.

Uyak, V., Akdagli, M., Cakmakci, M., & Koyuncu, I. (2014). Natural organic matter removal and fouling in a low pressure hybrid membrane systems. *The Scientific World Journal*, *2014*.

Van Bui, H., Grillo, F., Helmer, R., Goulas, A., & van Ommen, J. R. (2016). Controlled growth of palladium nanoparticles on graphene nanoplatelets via scalable atmospheric pressure atomic layer deposition. *The Journal of Physical Chemistry C*, *120*(16), 8832-8840.

Winter, J., Barbeau, B. and Bérubé, P. (2017). Nanofiltration and Tight Ultrafiltration Membranes for Natural Organic Matter Removal—Contribution of Fouling and Concentration Polarization to Filtration Resistance. *Membranes*, 7(3), p.34.

Appendix A Parameters of thickness-variety scenario

		LY5	LY6	LY7
ρ		998.19		
μ		0.0010016		
ΔP		3		
ε	ε_m	0.3		
	ε_s	0.3		
ε'	ε'_m	0.25		
	ε'_s	0.18	0.20	0.21
a_v	a_{vm}	$5.71*10^8$		
	a_{vs}	$1.47*10^9$	$1.33*10^8$	$1.25*10^8$
a'_v	a'_{vm}	$6.04*10^8$		
	a'_{vs}	$1.29*10^9$	$1.31*10^9$	$1.29*10^9$
τ	τ_m	1.826		
	τ_s	1.826		
τ'	τ'_m	1.986		
	τ'_s	2.354	2.20	2.173
l	l_m	$3.2*10^{-7}$		
	l_s(variable)	**$5.0*10^{-8}$-$1.2*10^{-7}$**		

where

ρ density of the fluid, kg/m^3

ε porosity of membrane, -

ΔP transmembrane pressure, bar

τ tortuosity factor, -

a_v specific surface area, $1/m$

μ viscosity of the fluid, $pa \cdot s$

l layer thickness, m

apostrophe represents the parameters after coating

subscript ‘m’ represents intermediate layer

subscript ‘s’ represents separation layer

Appendix B Parameters of Porosity-variety scenario

		LY5	LY6	LY7
ρ		998.19		
μ		0.0010016		
ΔP		3		
ε	ε_m	0.3		
	ε_s(variable)	**0.1-0.3**		
ε'	ε'_m	0.25		
	ε'_s	0.14	0.16	0.17
a_v	a_{vm}	$5.71*10^8$		
	a_{vs}	$1.47*10^9$-$3.82*10^9$	$1.33*10^9$-$3.44*10^8$	$1.25*10^9$-$3.23*10^8$
a'_v	a'_{vm}	$6.04*10^8$		
	a'_{vs}	$1.29*10^9$	$1.31*10^9$	$1.29*10^9$
τ	τ_m	1.826		
	τ_s	1.826-3.162		
τ'	τ'_m	1.986		
	τ'_s	4.078-2.354	2.220-3.844	2.173-3.763
l	l_m	$3.2*10^{-7}$		
	l_s	$5.0*10^{-8}$		

ρ density of the fluid, kg/m^3
ε porosity of membrane, -
ΔP transmembrane pressure, pa
τ tortuosity factor, -
a_v specific surface area, $1/m$
μ viscosity of the fluid, $pa \cdot s$
l layer thickness, m
apostrophe represents the parameters after coating
subscript ‘m’ represents intermediate layer
subscript ‘s’ represents separation layer